Ocean Engineering 142 (2017) 245–258

Contents lists available at ScienceDirect

Ocean Engineering

journal homepage: www.elsevier.com/locate/oceaneng

Numerical investigation of wave-induced vibrations and their effect on the fatigue damage of container ships

Fenglei Han*, Chunhui Wang, Ankang Hu

College of Shipbuilding Engineering, Harbin Engineering University, No. 145 Nantong Street, NanGang District, Harbin, Heilongjiang Province 150001, PR China

ARTICLE INFO

Keywords:
Wave-induced vibration
Springing
Whipping
Slamming
Seakeeping
Fatigue

ABSTRACT

Wave-induced vibrations of the ship hull girder consist of springing when it is associated with a resonance phenomenon, and whipping when it is caused by a transient impact loading due to wave slamming. This paper presents a new approach to predict the wave-induced vibrations and their contributions to fatigue damage of container ships. The seakeeping, whipping, springing and elastic modes calculations are coupled in every time step. According to the design characteristics of large container ships the existing methods are modified, air cushion effect and flow separation are considered in the slamming calculation, symmetric and asymmetric vibration modes equations are applied to predict the springing response in head seas and oblique seas. Based on rain flow counting method, spectral-based analysis method is used to calculate the additional fatigue damage due to springing and whipping.

1. Introduction

It is testified by full scale measurements in the Marine Accident Investigation Branch (2008) that the springing and whipping tend to increase the extreme stress, and the long term accumulative effect is the appearance of more critical fatigue damage. Storhaug et al., (2010, 2011) investigated the wave-induced vibrations and the consequence on fatigue of container ships through theoretical predictions, model tests and full scale measurements, in their research the results show that the contribution of vibrations to fatigue is up to 60% in bow quartering directions, the springing and whipping effects may dominate the fatigue loading.

The slamming induced whipping can be predicted taking into account the slamming force and the structural response, which is similar as the impact on seaplane floats during landing (Von-Karman, 1929; Wagner, 1931), this process can be simplified as a wedge water entry problem, based on Von-Karman's theories Wagner applied flat plate fitting hypothesis to calculate the wet half width considering the existence of free surface bulge, in this way the added mass, impact force and the pressure distribution are solved more accurately. On guidance of Wagner's flat plate fitting method Bisplinghoff and Doherty (1952) and Fabula (1957) proposed “diamond fitting” and “ellipse fitting” approximation solutions, but in practice the shapes of the body surface of the ships are arbitrary, and the approximate solutions are not applicable. With the improvement of computer ability Zhao et al. (1996) adopted numerical analysis in 2-D arbitrary section to solve entry water problem, in which the higher order terms of the pressure is computed according to the nonlinear Bernoulli equation, the original Wagner model overestimates the slamming force, especially when the dead rise angle is large, so Generalized Wagner Model (GWM) is more accurate in terms of slamming prediction. Moctar et al. (2017) proposed a Reynolds-averaged Navier-Stokes (RANS) equations coupled with the nonlinear rigid body motion equations to assess the slamming-induced hull whipping on sectional loads of three containerships. Through full scale measurements and experiment, Kahl Adrian et al.(2014) investigated the fatigue damage due to low and high frequency loads. Rahaman and Akimoto (2012) developed a CFD method to predict the slamming on bow flare of container ships by visualization technique. Zhu and Moan (2013) estimated the wave-induced nonlinear effect of vertical load effect for container ships considering higher order harmonics to achieve the balance between regular and irregular waves.

How to deal with the jet flow on the contact point between free surface and body surface is a difficult problem, as shown in Fig. 1. When the slamming section is blunt the jet flow will separate from the body, if the section is concave the jet flow will not separate from the body, so when the separation appeared the jet flow should be truncated in the contact region. Dobrovolskaya (1989) proposed a different numerical calculation method, the 2-D body is considered as wedge including the top of the body, the velocity is constant, and the flow field

* Corresponding author.
E-mail address: fenglei_han@163.com (F. Han).

http://dx.doi.org/10.1016/j.oceaneng.2017.06.064
Received 21 March 2016; Received in revised form 27 June 2017; Accepted 27 June 2017

Nomenclature

φ	the velocity potential
S_B	the wetted body surface between points A and C
S_F	the free surface outside points B and D
p	the pressure on the body surface
S_∞	the a control surface far away from the body
S	including S_B, S_F, and S_∞
p_0	the atmospheric pressure
β	the dead rise angle
ρ	the mass density of the fluid
p_s	the slamming pressure
N_{sec}	the total section number
N_{slam}	the total number of slamming sections
f_s	the modal excitation force by the slamming pressure
S_b	the contour of the section
h_s	the integral over the width of the section
n	the normal vector of the hull surface
p(x,t)	the pressure distribution along the wetted part
$\phi(x,t)$	the velocity potential in the contact region
f(x)	the function of the body shape
h(t)	the prescribed penetration depth
C_{air}	the coefficient of the relationship between the sound velocity and the pressure in air cushion
γ	the adiabatic ratio
ρ_1	the air density
C_0	the sound velocity under pressure p_0
A	the plate area of unite length
V_0	the initial velocity
g	the acceleration of gravity[9.81 m/s^2]
w_l (x,t)	the relative displacement between the section and the wave
$\xi(x,t)$	the wave elevation
w(x,t)	the vertical displacement of the section
N(x)	the damping coefficient
B(x)	the strip width
H(x)	the kinematic force
F(x, t)	the wave-induced force
$p_r(t)$	is the r-order dry mode principle value
w_r	the r-order displacement
μ	the unit mass,
Iy	the moment of inertia
θ_r	the r-order angle of torsion
νr	the damping coefficient
A_{rs}	the generalized fluid mass
B_{rs}	the generalized fluid damping
C_{rs}	the generalized fluid stiffness;
ω_e	the encounter frequency
M(x,t)	the bending moment of time domain
V(x,t)	the shear force of time domain
Π	the wave excitation force amplitude matrix
$G_{\eta\eta}$	the power spectral density of the wave
H_s	the significant wave height
T_z	zero-crossing period
T_d	the fatigue life
D	the accumulate fatigue damage degree;
N_{load}	the loading number
P_n	the n-th loading state proportion
$\Gamma(1+m/2)$	the gamma function
n_s	the sea state number
n_H	the total number of heading angles
p_i	the i-th sea state probability
p_j	the j-th heading angle probability
m_0	the zero order moment
ν_{ijn}	the alternating stress average crossing zero probability
Ω	the fluid domain

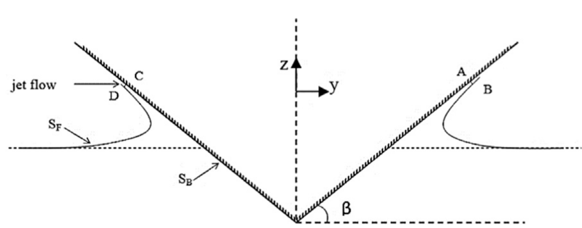

Fig. 1. Definition of values and control surface in the calculation of slamming.

is characterized as self-similarity. Based on analysis of fixed pressure condition and kinematic condition, the problem is transformed into a nonlinear singular integral equation, so as to obtain the pressure distribution using clear expression of complex velocity potential. Dobrovolskaya presented the numerical calculation when the dead rise angle $\beta \geq 30°$, based on her research Zhao and Faltinsen (1993) made further efforts to expand the calculation with $\beta = 4–81°$, the results are very close to the asymptotic solutions considering the jet flow. Faltinsen (1999) generalized Wagner's model to solve wedges of small dead rise angle with orthotropic plates.

Under-approximation of flat-disc Vorus (1996) used nonlinear dynamic free surface condition and nonlinear Bernoulli equation to calculate the impact force, and Logvinovich (1969) mentioned that the original Wagner model is not valid on the contact points, and suggested that an additional term should be added to the velocity potential, which is calculated under the condition that the velocity at the point where the pressure is equal to zero is double that of the contact point. Korobkin (2004) modified Logvinovich model, the potential on the body boundary is calculated by Taylor expansion, and the pressure on the body is computed by nonlinear Bernoulli equation. Tassin et al., (2013, 2014) developed the method to analyze the symmetric body whose shape varies in time, and with flow separation and cavity initiation. The other kind of models are applied to make the method valid in different concrete situations (Khabakhpasheva et al., 2013; Korobkin, 2003, 2006; Semenov, 2009), such as ventilation, aeration, and cavitation and so on.

In the impact process the air cushion effect is neglected, but when $\beta \leq 3°$ the air cushion affects the slamming force and response duration significantly according to Chuang's (1966, 1970) research. In 1970 Chuang deduced the equations to predict the pressure of flat plate impact considering air cushion effect through a series of experiments, the experimental results show that when $\beta = 0–1°$, small volumes of air are captured into the interlayer between the water and the body in the duration of impact, when $\beta > 3°$ the air escapes quickly and the volumes are very small, the effect is not significant.

For marine structures the fluid induced vibrations are the main fatigue source, except the wave-induced vibration the vortex-induced vibration is a main cause of fatigue too. Gu and Duan (2016) investigated the vortex-induced vibration through Generalized Integral Transform Technique (GITT) using experimental data as input. Wang and Xiao (2016) observed the single-mode in-line (IL) and cross-flow (CF) vibrations, and presented the importance of the fatigue damage due to IL in the design of low flow velocity. The other scholars also assessed the fatigue damage of flexible cylinders due to vortex-induced vibrations (Zheng et al., 2014; Rao et al., 2015; Park and Song, 2015; Hsieh et al., 2017), which is very important for the structure design.

Springing and whipping theories are clearly put forward relatively late, springing phenomenon was observed in the early 60's of the 20th century, and from then on the increase of vertical bending moment and stress response induced by continuous wave pressures attracted more and more attention of scholars. Cleary et al. (1971) firstly identified the main source of fatigue damage for the Great Lakes ship as springing. Belgova (1962) revealed the excitation sources of springing through experiments. Storhaug (2007) in his dissertation proposed the principle to calculate the wave-induced 2-node vertical vibration, which is testified by model tests and full scale measurements, and the additional fatigue damage caused by springing and whipping is computed, according to this research the contribution of wave-induced vibrations to total fatigue damage for a 300 m iron ore ship is up to 44% in the North Atlantic seas, and vibrations in the ballast condition are larger than in the cargo condition. Miyake et al. (2010) gave a numerical analysis of hydroelastic response including whipping and springing for ultra-large container ships, the results are compared with experiment data to verify that the applied nonlinear strip method is applicable for estimating the hydroelastic responses. Fricke and Paetzold (2014) discussed the whipping effect on container ships through fatigue tests comparison with and without whipping load, so as to present the whipping contribution to fatigue damage. Kahl et al. (2013) and Eggert et al. (2012) assessed cumulative fatigue damage of container ships due to high-frequency response operating in North Atlantic and North Pacific seaways. Moctar et al. presented a computational method to assess the whipping on sectional loads considering the second order Stokes waves and nonlinear wave fields through the solution of nonlinear Schrodinger equations.

The wave-induced response can be predicted through experiments. Drummen et al. (2008) gave a comparison between shot-term probability distribution and random irregular waves experimentally, and they found that the results from conditioned waves and from random irregular waves are consistent for the rigid hull, for flexible hull the results from conditioned waves are lower than random irregular wave results. Zhu and Moan (2013) presented a model tests of an 8600TEU and 13000TEU container ships, in which the second and third harmonics are analyzed in detail.

In this paper the theories and numerical calculations are generalized to be applicable for large container ships, the bow section of large container ship includes big flare, flat bottom and bulb, so in the 2-D slamming calculation the shapes of the 2-D sections should be modified, and according to the different modified shapes different methods are applied to satisfy the hypothesis. In the bottom slamming calculation the air cushion effect is considered when the rise angle of the boundary element $\beta < 3°$. In the whole process, the 3-D frequency seakeeping, springing, slamming calculations are coupled, the structure responses are obtained directly through loading the wave pressures on the whole finite element model. The fatigue damage is assessed by spectral analysis according to sea conditions and loading conditions, the assessment process is shown in Fig. 2 in detail.

2. Slamming calculations

In order to calculate the diffraction and radiation forces the hydrodynamic coefficients are obtained by solving the boundary value problem using the potential flow theory in the frequency domain. 3-D Rankine Panel Method is applicable in seakeeping prediction, the calculation is completed by an in-house program based on Nakos's (1990) work, and the difference is that the velocity potential is calculated as unit amplitude velocity potential in the concrete computation.

2.1. Generalized Wagner Model (GWM)

How to use Wagener method to calculate the arbitrary sections water entry problem proposed by Zhao and Faltinsen. In this paper a boundary element method is used to deal with the slamming problem, for every segment a line element linearization calculation is applied, in which the jet flow with and without separation is considered.

The fluid is assumed to be incompressible and ideal, so that the Laplace equation is satisfied, the free surface condition and the body surface condition are satisfied too. Jet flow is generated between the free surface and body surface, the jet flow is cut at AB and CD, as shown in Fig. 1. The fluid domain is Ω, which consists of AB, CD, S_B, S_F and S_∞. According to Green's second identity, the velocity potential in the fluid field can be expressed as:

$$2\pi\varphi(y, z, t) = \int_S \left[\frac{\partial\varphi(\eta, \xi, t)}{\partial n(\eta, \xi)} logr - \varphi(\eta, \xi, t)\frac{\partial logr}{\partial n(\eta, \xi)}\right] ds((\eta, \xi, t) \tag{1}$$

In the above equation $r = \sqrt{(y-\eta)^2 + (z-\xi)^2}$, surface S consists of AB, CD, wet body surface, free surface and control surface far away from body, (η, ξ) is the body fixed coordinates. Due to the symmetry of the ship, the jet can be regarded as the vertical dipole in the infinite fluid field. In the numerical computation the free surface and body surface is meshed into boundary line elements, on the contact region fine mesh is necessary for improving the accuracy because of the quick changing potential, the mass particles are integrated over time, the contact point is computed to obtain the wet surface position.

Using Bernoulli's equation to solve the pressure on every line element, the pressure expression is:

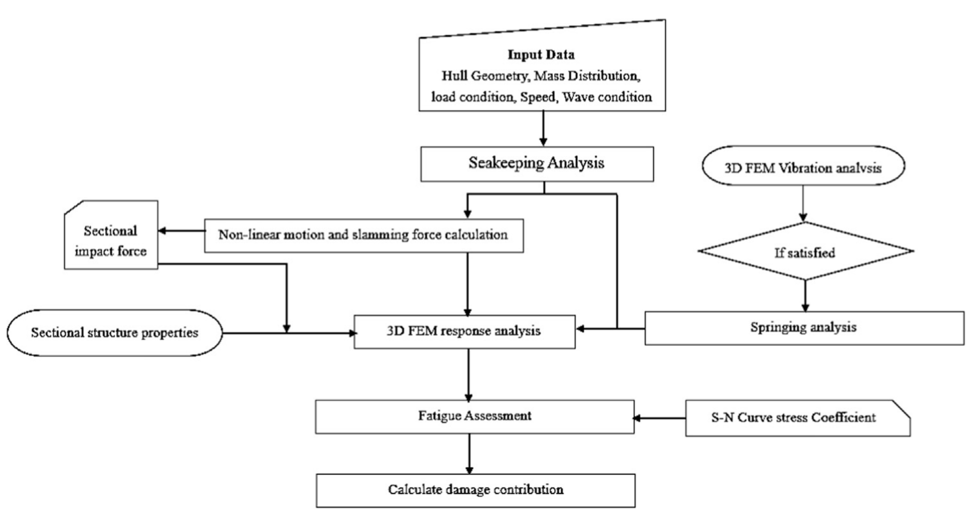

Fig. 2. Fatigue assessment procedure.

$$P_i - P_0 = -\rho\frac{\partial\varphi_i}{\partial t} - \frac{1}{2}\rho\left[\left(\frac{\partial\varphi_i}{\partial y}\right)^2 + \left(\frac{\partial\varphi_i}{\partial z}\right)^2\right] \tag{2}$$

After every element is solved, the slamming pressure is calculated by integration along the cross section.

$$p_s = 2\int_{S_b} P\bullet nds = 2\sum_i^{N_{sec}} P_i\bullet n_i dl_i \tag{3}$$

where N_{sec} is the total section number, N_{slam} is the number of slamming sections, after getting the slamming pressure of each section, the modal excitation force by the slamming pressure can be calculated by the integral along the global ship:

$$f_s = 2\sum_{i=1}^{N_{slam}}\int_{S_b} p_s\bullet h_s dl \tag{4}$$

2.2. Modified Logvinovich model (MLM)

Logvinovich model is established based on the Wagner flat plate fitting model, in the adjacent area of the contact point where the pressure reaches the maximum value Wagner method is not valid. At the same time only when the pressure obtained by nonlinear Bernoulli equation is positive the Wagner model is valid, so Logvinovich (1969) proposed that an additional term is added to the velocity potential distribution, thus the potential is bounded in the contact area. On the basis of Lognovich theory, Korobkin (2004) retains the high order terms of the body surface condition in the Bernoulli equation; through this procedure this method can be widely applied.

The pressure p(x, t) is distributed along the wet surface D(t), when the potential and wet area are known, the expression can be rewritten as:

$$\phi(x, t) = \varphi(x, f(x) - h(t), t) \tag{5}$$

By Cauchy-Lagrange integral equation:

$$p(x, y, t) = -\rho\left(\varphi_t + \frac{1}{2}|\nabla\varphi|^2\right) \tag{6}$$

The body surface condition is written as follows:

$$\varphi_y = \varphi_x f'(x) - \dot{h}(t) \tag{7}$$

The pressure is expressed as:

$$p(x, t) = -\rho\left[\varphi_t + \frac{f'(x)\dot{h}}{1+f^2(x)}\phi_x + \frac{1}{2}\frac{\phi_x^2 - \dot{h}^2}{1+f^2(x)}\right] \tag{8}$$

2.3. Air cushion effect in water impact

In the slamming calculation the dead rise angles are assumed to be greater than 3°, but for containerships the bow section lines are irregular. Some of the rise angles of the line elements are not greater than 3°, according to Chuang's (1966) research, the air cushion effect should be considered.

In the water entry process some air is captured into the interlayer between the body and the water surfaces, and the air water mixture is generated, which will decrease the impact force, the duration time cannot be neglected. The time pressure increasing from zero to the maximum value is 2 L/C_{air}, where L is the half width of the plate, C_{air} is the coefficient of the relationship between the sound velocity and the pressure in air cushion, here C_{air} is equal to the speed of sound in the trapped air, the air compressing process is isentropic, the following equation is tenable:

$$\frac{p}{P_0} = \left(\frac{\rho_1}{\rho_0}\right)^{\gamma} \tag{9}$$

Where ρ_1 is the air density under the pressure p, ρ_0 is the air density under the standard atmospheric pressure p_0, γ is adiabatic ratio, and generally γ equal to 1.4:

$$\frac{dp}{d\rho_1} = C_{air}^2 \tag{10}$$

This equation is derived leading to:

$$\frac{p}{p_0} = \left(\frac{C_{air}}{C_0}\right)^{\frac{2\gamma}{\gamma-1}} \tag{11}$$

$$C_{air} = C_0\left(\frac{p_0 + p}{p_0}\right)^{\frac{\gamma-1}{2\gamma}} \tag{12}$$

C_0 is the sound velocity under pressure p_0, through above analysis pressure wave propagation distance is:

$$\int_0^{4L} dl = \int_0^T c_{air}dt \tag{13}$$

Pressure impulse attenuation form is:

$$p(t) = 2p_{max}e^{-1.4t/T}sin\pi\frac{t}{T} \tag{14}$$

Through the above calculation formula, it can be seen that the pressure is a sine function with constant amplitude, which can be obtained by the uniform distribution hypothesis and the momentum theorem:

$$mV_0 = A\int_0^T 2p_{max}e^{-1.4t/T}sin\pi\frac{t}{T}dt \tag{15}$$

The added mass of the plate $m = \frac{1}{2}\rho\pi L^2$, which is substituted into (15):

$$\frac{1}{2}\rho\pi L^2 V_0 = A\int_0^T 2p_{max}e^{-1.4t/T}sin\pi\frac{t}{T}dt \tag{16}$$

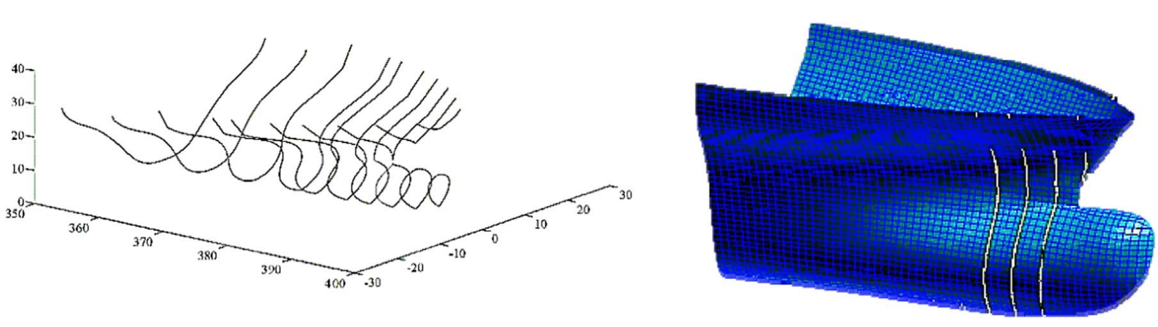

a) Bow cross section lines
b) Bow finite element model

Fig. 3. Bow cross section lines and finite element model of containership.

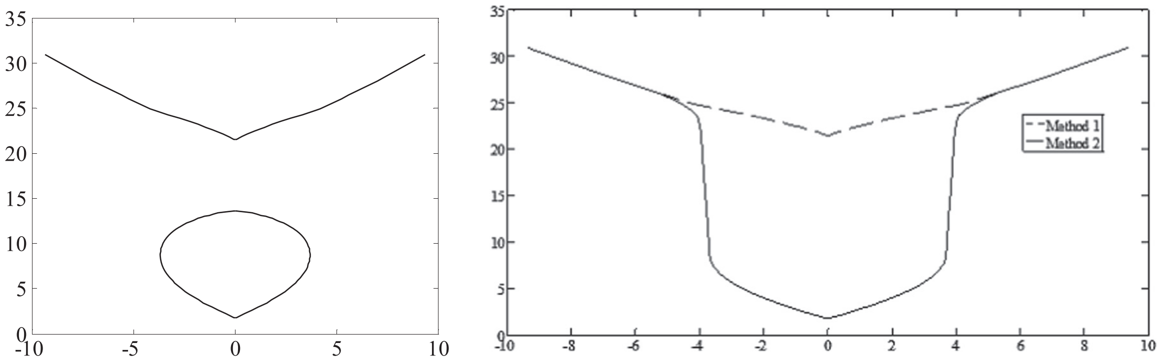

a) Original shape b) Modified shapes

Fig. 4. Modification to the shapes of the cross sections.

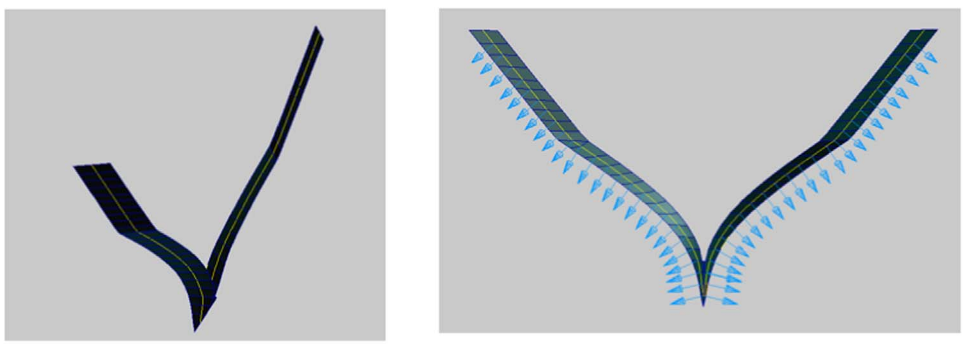

a) Slamming section without loading b) Slamming section with loading

Fig. 5. Single slamming section inserted into finite element mod.

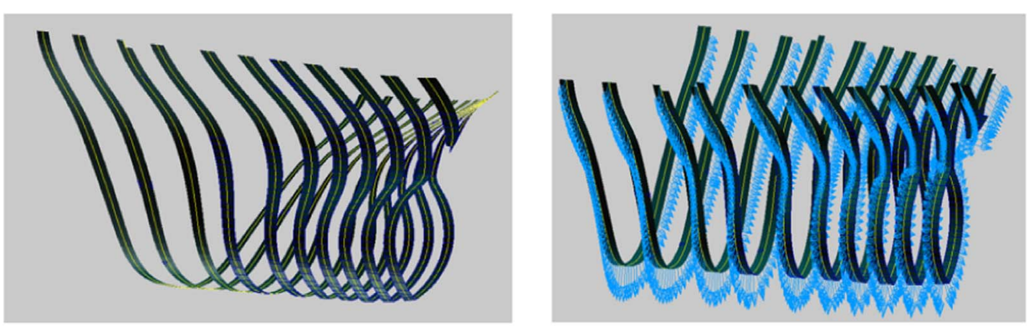

a) Slamming cross sections without loading b) Slamming cross sections with loading

Fig. 6. Slamming calculation sections inserted into finite element model.

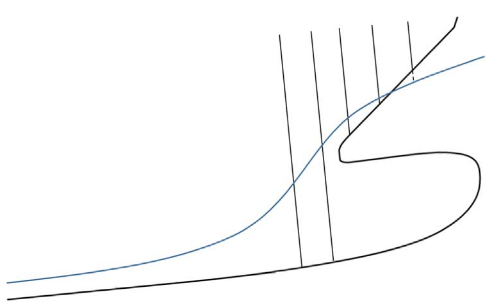

Fig. 7. Relative motion calculation.

A is the plate area of unite length, substitute (15) and (6) into (16):

$$4L = C_0\left(\frac{1}{p_0}\right)\int_0^T\left(p_0 + 2p_{max}e^{-1.4t/T}sin\pi\frac{t}{T}\right)^{\frac{1}{7}}dt \tag{17}$$

Using (16) and (17) the following equation is obtained:

Table 1
Principal dimensions of 16000TEU container vessel.

Length (O.A.)	396.0 m
Length (B.P.)	379.0 m
Hull Breadth	54.0 m
Hull Depth	30.2 m
Design Draft	14.5 m
Scantling Draft	16.0 m
Service Speed	22.5 kn

$$p_{max}=16.63V_0^{1.1} \tag{18}$$

In the numerical computation the pressure integral function is:

$$p_s = \int_{S_b} P\bullet nds = 2\sum_{i=1}^{k} p_{max}\sqrt{(y_{i+1}-y_i)^2+(x_{i+1}-x_i)^2} + 2\sum_{i=k+1}^{N_{sec}} P_i\bullet n_i dl_i \tag{19}$$

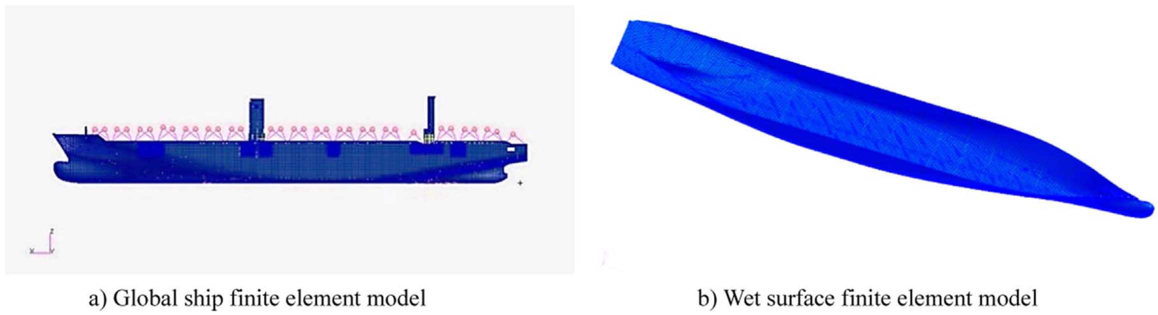

Fig. 8. Finite element model for modal analysis.

Table 2
Vibration calculation results.

Mode	Loading condition	Vertical			Torsion	Horizontal		
		1 mode	2 mode	3 mode	1 mode	1 mode	2 mode	3 mode
Dry mode	Ballast	0.602	1.135	1.724	0.528	0.655	1.244	1.679
	Full load	0.703	1.308	1.854	0.623	0.957	1.686	2.402
Wet mode	Ballast	0.521	0.986	1.523	0.412	0.531	0.975	1.417
	Full load	0.581	1.098	1.672	0.513	0.816	1.478	2.147

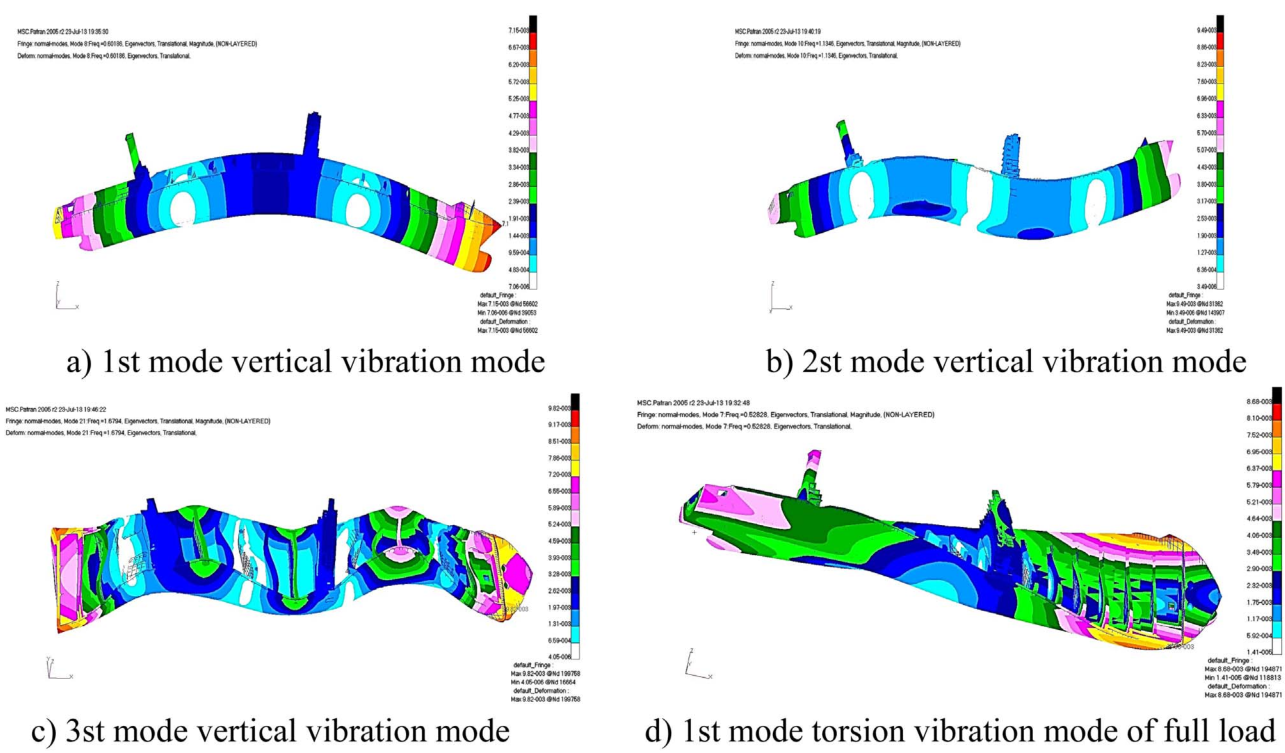

Fig. 9. Dry mode vibration nephograms of full load condition.

Table 3
Sea states of 25 years occurrence period.

T_z (s)	4	4.5	5	5.5	6	6.5	7	7.5	8
H_s (m)	1.7	2.9	4.2	5.6	7	8.4	9.6	10.8	11.8
T_z (s)	8.5	9	9.5	10	10.5	11	11.5	12	12.5
H_s (m)	12.6	13.4	14	14.5	14.8	15.1	15.3	15.4	15.3
T_z (s)	13	13.5	14	14.5	15	15.5	16	16.5	17
H_s (m)	15.2	15	14.7	14.4	13.9	13.2	12.4	11.4	9.7

3. Springing calculations

The relative displacement between the section and the wave is

$$w_l(x,t) = w(x,t) - \xi(x,t) \tag{20}$$

where w(x,t) is vertical displacement of the section, ξ(x,t) is wave elevation, according to strip theory the symmetric force is as follows:

$$z(x,t) = -\left\{\frac{D}{Dt}\left[m(x) + \frac{i}{\omega_e}N(x)\right]\frac{Dw_l(x,t)}{Dt}\right\} + \rho g B(x) w_l(x,t) \tag{21}$$

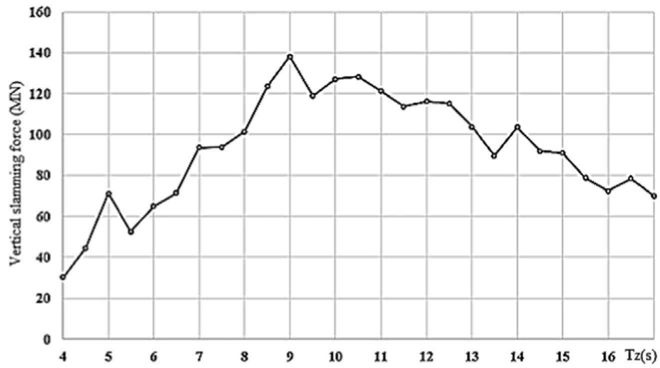

Fig. 10. Vertical slamming force amplitude in different sea states.

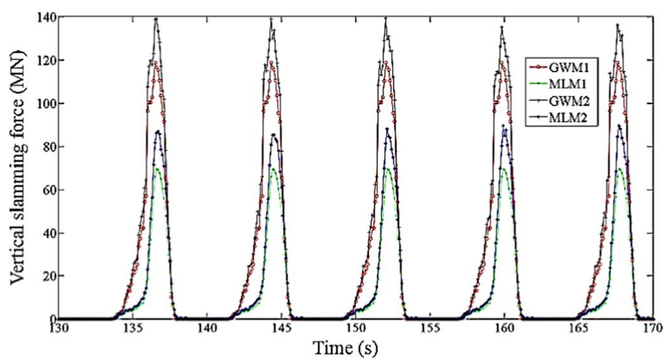

Fig. 11. Vertical slamming force calculation in time domain by two methods.

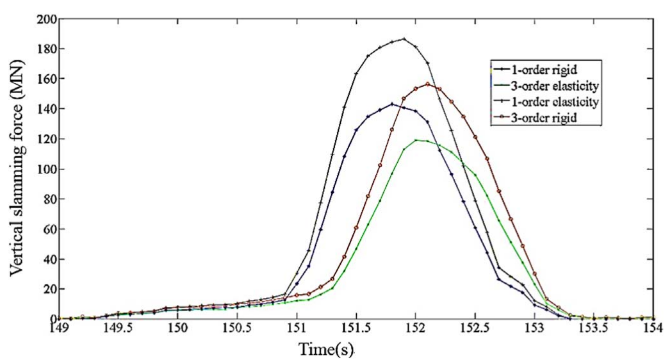

Fig. 12. Influence of hydroelasticity.

In above equation D/Dt is material derivative. m(x) is section mass; N(x) is damping coefficient; B(x) is strip width;

The fluid force is divided into kinematic force H(x) and wave-induced force F(x, t):

$$H(x,\,t) = \left[m(x) + \frac{iN(x)}{\omega_e}\right]\frac{D^2w(x,\,t)}{Dt^2} - V_0\left[m'(x) + \frac{iN'(x)}{\omega_e}\right]\frac{Dw(x,\,t)}{Dt} + \rho gB(x,\,t)w(x,\,t) \tag{22}$$

$$F(x,\,t) = \left[m(x) + \frac{iN(x)}{\omega_e}\right]\frac{D^2\xi(x,\,t)}{Dt^2} - V_0\left[m'(x) + \frac{iN'(x)}{\omega_e}\right]\frac{D\xi(x,\,t)}{Dt} + \rho gB(x,\,t)\xi(x,\,t) \tag{23}$$

$p_r(t)$ is the r-order dry mode principle value, the vertical displacement of the ship hull is represented as the sum of the displacement of each mode:

$$w(x,\,t) = \sum_{r=0}^{\infty} p_r(t)w_r(x) \tag{24}$$

The generalized fluid force can be written as the following two parts:

$$H_r(t) = \int_0^l H(x,\,t)w_r(x)dx \tag{25}$$

$$\Pi_r(t) = \int_0^l F(x,\,t)w_r(x)dx \tag{26}$$

The fluid force is brought into the symmetric vibration equation:

$$a_{ss}\ddot{p}_s(t) + a_{ss}\omega_s^2 p_s(t) + b_{ss}\dot{p}_s(t) + \sum_{r=0}^{\infty} A_{rs}\ddot{p}_r(t) + B_{rs}\dot{p}_r(t) + c_{rs}p_r(t) = \Pi_s e^{-i\omega_e t} \tag{27}$$

where $a_{ss} = \int_0^l (\mu w_r^2 + I_y\theta_r^2)dx$, $c_{ss} = \omega_s^2 a_{ss}$, $b_{ss} = 2a_{ss}\omega_s\upsilon_s$, μ is unit mass, I_y is moment of inertia, damping coefficient is calculated by empirical formula $\upsilon_s = 7.3\times10^{-3}\omega_r$.

A_{rs} is generalized fluid mass; B_{rs} is generalized fluid damping; C_{rs} is generalized fluid stiffness;

By solving the above differential equations, the principal values are obtained, the hull displacement is the sum of the displacement components of each mode, the displacement, bending moment and shear force of time domain are computed as the following equations:

$$w(x,\,t) = e^{-i\omega_e t}\sum\nolimits_{r=0}^{n} p_r w_r(x) \tag{28}$$

$$M(x,\,t) = e^{-i\omega_e t}\sum\nolimits_{r=0}^{n} p_r M_r(x) \tag{29}$$

$$V(x,\,t) = e^{-i\omega_e t}\sum\nolimits_{r=0}^{n} p_r V_r(x) \tag{30}$$

In oblique seas the vibration function should be modified, the vibration is asymmetric, the wave change in the width direction must be considered, and the asymmetric vibration function can be written as matrix form:

$$[(c + C) - \omega_e^2(a + A) - i\omega_e(b + B)]p = \Pi \tag{31}$$

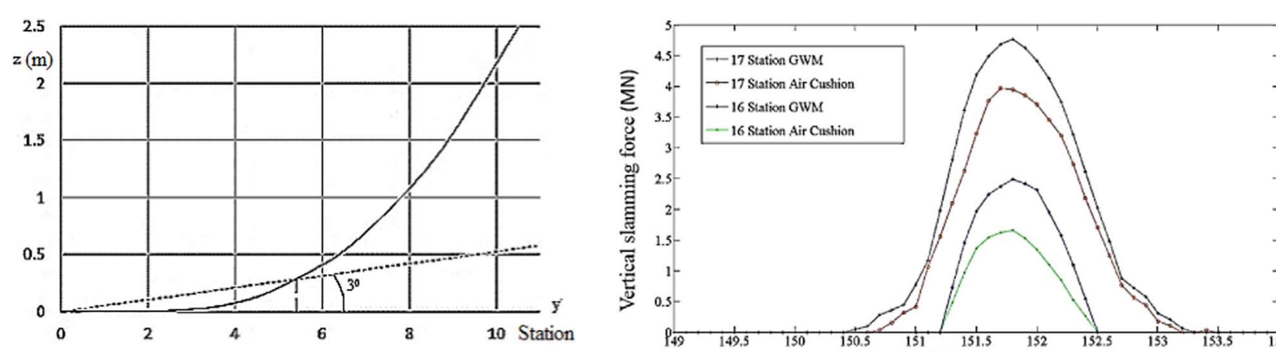

a) Air cushion effect position　　b) slamming force calculated with and without air cushion effect

Fig. 13. Air cushion effect

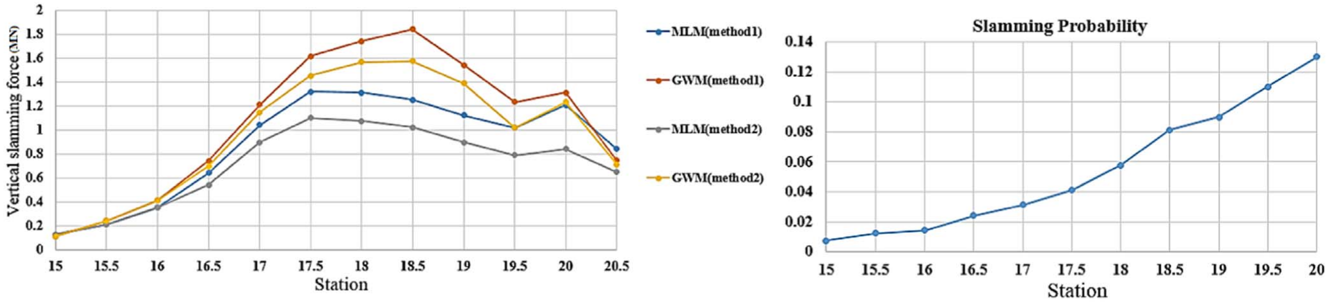

a) Vertical slamming force at different stations

b) Slamming probability at different stations

Fig. 14. Verification of slamming effect.

a is dry mode generalized mass matrix; c is dry mode generalized stiffness matrix; b is dry mode generalized damping matrix; A is fluid added mass matrix; B is fluid damping matrix; C is fluid stiffness matrix; Π is wave excitation force amplitude matrix;

By solving algebraic equations the complex solution of the principle values p is obtained, based on which the time domain bending moment and torsion can be calculated.

4. Pressure integral calculation

4.1. Section geometry modification

For container ship the bow cross sections are irregular shapes, as shown in Fig. 3, which do not conform to the assumptions of 2-D slamming calculation, so the shapes should be modified to be consistent with the assumptions. The finite element model shown in Fig. 3 is established by FEM software MSC.Patran. There are two methods to deal with the bulb, one is to delete the bulb, and another way is to modify the two part into one, as shown in Fig. 4, and the curve is smoothed at the angle where the slope is discontinuous. In method 2 the bottom of the bulb shape keeps original to make the entry water calculation be accurate.

This modification approach is proposed by Hermundstad and Moan (2005), which is also applied by Kim et al. (2015), and the vertical slamming force comparison is presented in their work. In order to clarify the difference between two modified geometries, the slamming probability and force of different stations are compared to indicate the difference of calculation results.

4.2. Pressure integration

The slamming sections are inserted into the finite element model to obtain the structure response, and the vibration calculation is based on the finite element model too, so the calculations are possible to be consistent with each other. The wave pressures which are calculated by the modified cross sections should be mapped to the real structure model, as shown in Fig. 5, and in order to improve the accuracy more sections are used, the finite element model with and without wave pressures loading are shown in Fig. 6.

The excitation force is the integral of the slamming pressure along 3-D mesh:

$$f_s = \sum_{i}^{N} p_s \bullet h \bullet ndS \tag{32}$$

N is the total number of the slamming calculation sections, p_s is slamming force, S is the section surface. This equation is transformed into line integration function:

$$f_s = \sum_{i=1}^{N} \int_L p_s \bullet h_s dl \tag{33}$$

Where the $h_s(l)$ is pre-calculated by vibration modal analysis, L defines the section contour. Because the vibration mode is steady along the section contour, so the value is unchanged in every time step.

$$\boldsymbol{h}_s(l)dl = h\int \boldsymbol{n}dw \tag{34}$$

The right hand of above equation is over the width of the section. The slamming calculation should be coupled with the seakeeping program, when the slamming section is merged into the water and the relative motion exceeds the defined limit, the coupling calculation starts to perform. The relative motion is obtained from the longitudinal plane of the ship and the wave profile using Rankine panel seakeeping program, when it exceeds the threshold defined by user and the immersion of the section is above zero, as shown in Fig. 7, the slamming calculation is initialized. When the relative velocity drops below a defined limit the slamming calculation is stopped.

5. Calculation results and comparisons

A 16000TEU container ship is used to illustrate the computational difference; the principal dimensions are given in Table 1 as below:

5.1. Vibration modal analysis

The three dimensional finite element model is shown is Fig. 8, the wet surface is defined to calculate the added mass of the different loading conditions, this procedure is completed in FEM software MSC.Patran.

The calculation results are given in Table 2.

The dry mode vibration nephograms of full load condition are shown in Fig. 9.

5.2. Slamming calculation results and comparison

In the short-term approach, the sea states that occur once in 25 years are selected, which is presented in Table 3. Short term predictions and extreme value analysis show that when the zero-crossing period is 9 s and the significant wave height is 13.4 m the slamming force amplitude reaches the maximum value, as shown in Fig. 10. For verification of the calculation method, this condition is selected to explain the difference between the different methods. The calculation speed is 22.5 kn, which is equal to the service speed of this 16000TEU container ship.

The slamming force is calculated by Generalized Wagner Model (GWM) and Modified Logvinovich Model (MLM), as shown in Fig. 11. The results obtained from MLM are smaller, the reason of this difference is that the MLM requires the cross section shape to be

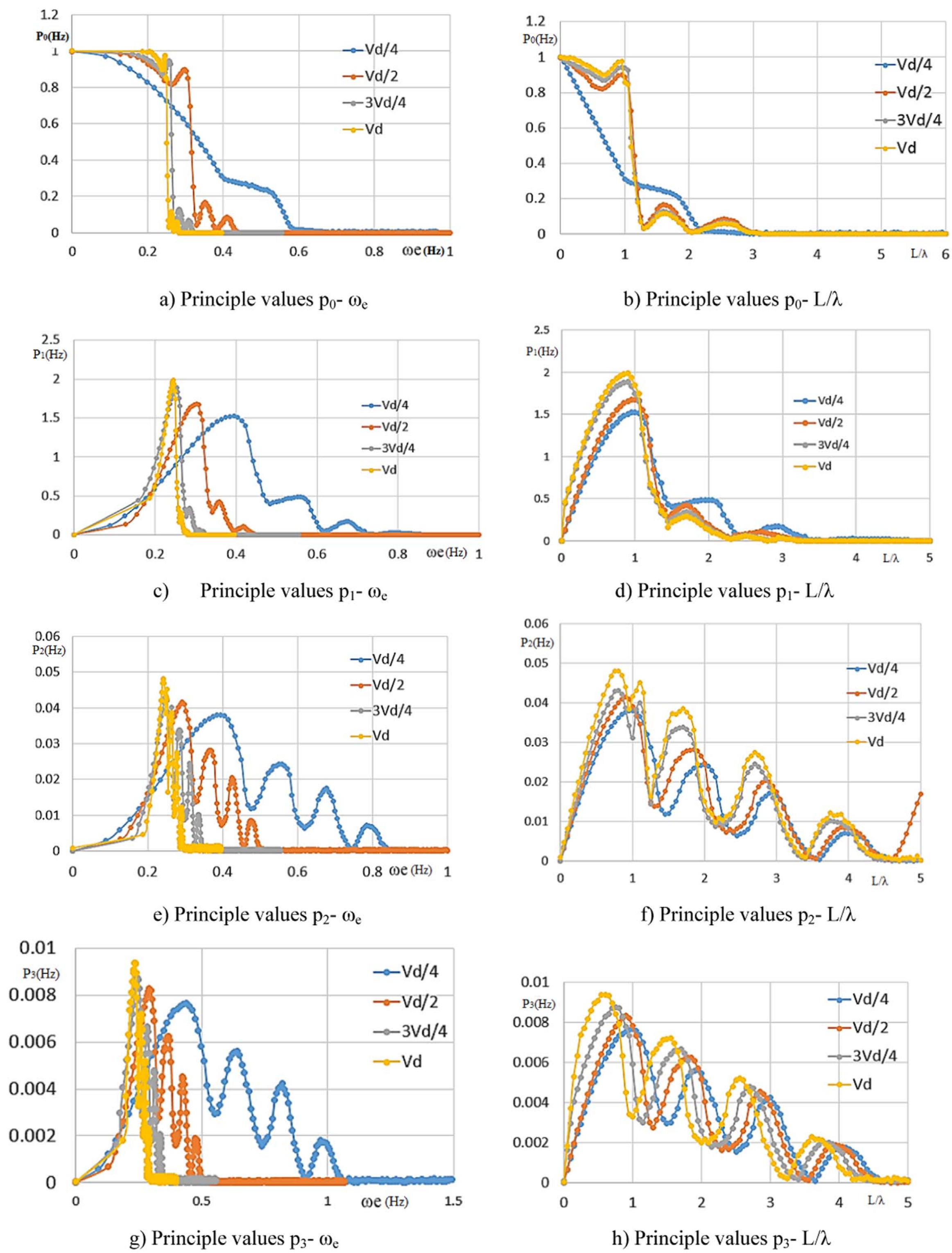

Fig. 15. Variation of principle values.

blunt, but for container ship some of the sections are not blunt, especially for the sections above the bulb. It is obvious that the results calculated by method 2 are larger than method1. MLM is much faster than GWM, because the sections are blunt in method2, so that the MLM can be reasonably used in the computation.

The duration of slamming impact is about 1 s, and considering the wet frequency it is about 1.6 s, the effect of hydroelasticity is obvious in the process (Bereznitski, 2003), due to the structure damping the slamming will decrease gradually. If the ship hull elasticity is assumed to be rigid body, the slamming force will increase significantly, when the modes order increasing the result is going to be convergent. In the calculation considering the hydroelasticity the slamming and seakeeping programs are coupled, the rigid body displacement is taken into account in the coupled programs, the comparison is shown in Fig. 12.

On the 16-th and 17-th stations, when $y < 5.36$ m the dead rise angle $\alpha < 3°$, this part is computed as a plate entry water problem, the line element is divided at this point. By comparing the results calculated by GWM considering and not considering the aircushion

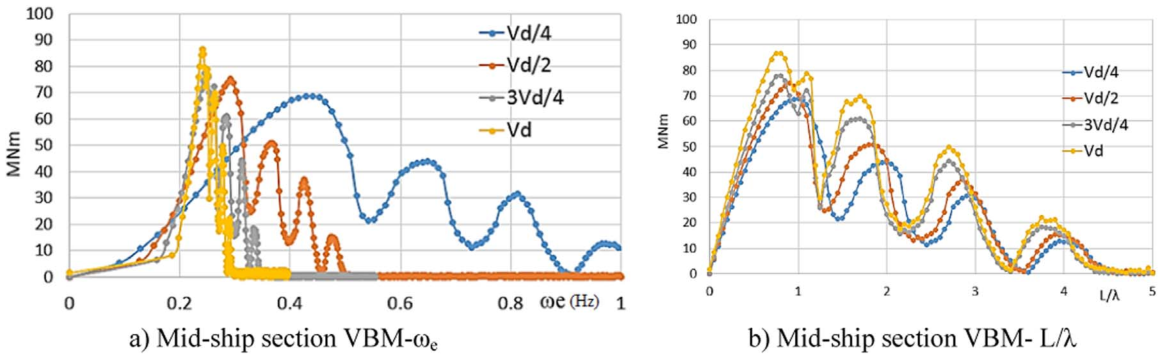

Fig. 16. Vertical bending moment in mid-ship section.

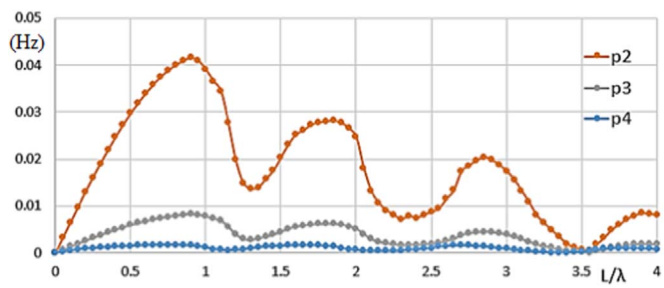

Fig. 17. Principle values in low frequency domain.

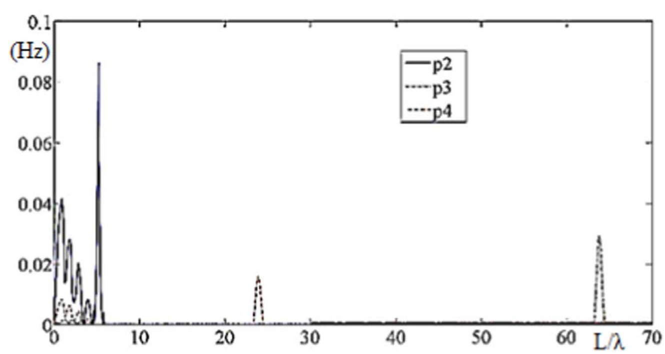

Fig. 18. Principle values in high frequency domain- L/λ.

effect, it is obvious that the air cushion can reduce and delay the slamming impact force, the differences are shown in Fig. 13.

Although air cushion effect is identified clearly in some sections, but for the pressure integration of the global ship the difference is not large, which is because the air cushion is generated in a very small area, in this case only in the 16th and 17th stations the air cushion should be considered.

To verify the bottom slamming and the flare slamming effects, the results of station 15–20 are shown in Fig. 14; the vertical slamming force is higher when the section is close to the bow before 18.5 station, and then the forces decrease. But the slamming probability is much higher when the section is close to the bow as shown in Fig. 14(b). Based on this analysis the flare slamming is more serious in the bow slamming prediction, even if the bottom slamming is also considerable in this part.

5.3. Springing calculation results

Here the springing symmetric response results of different heading speeds are given, the design speed of this 16000TEU container ship V_d = 22.5 kn, in this section four speeds are calculated $3V_d/4$, $V_d/2$, $V_d/4$ and V_d, the principle values changing with the encounter frequency and the ratio of wave amplitude to the ship length are given in Fig. 15.

As shown in Fig. 15, with the increasing of the heading speed, the principle values become larger, when the wavelength is equal to the ship length there is a small peak value of p_0 and p_1, two peak values of p_2 exist on the both sides of $L/\lambda = 1$, L is the ship length, λ is wavelength, so L/λ is dimensionless, the unit is arbitrary unit 1.

The midship bending moment has great influence to the fatigue damage, here we calculate the variation curves of mid-ship bending moment, which are shown in Fig. 16:

From the VBM variation we can see that in the calculation of bending moment p_2 plays a leading role, VBM variation trend is consistent with the calculated results of p_2, as shown in Fig. 17.

The springing response can be predicted through principle values and Vertical Bending Moment (VBM) analysis on broad band frequencies, the values of peak values of p_2, p_2 and p_4 locate at $\omega_e = 0.534$, $\omega_e = 0.984$ and $\omega_e = 1.511$, as shown in Fig. 18, these points are very close to the wet natural frequencies which are calculated from modal analysis by finite element method, which is consistent with the theory analysis.

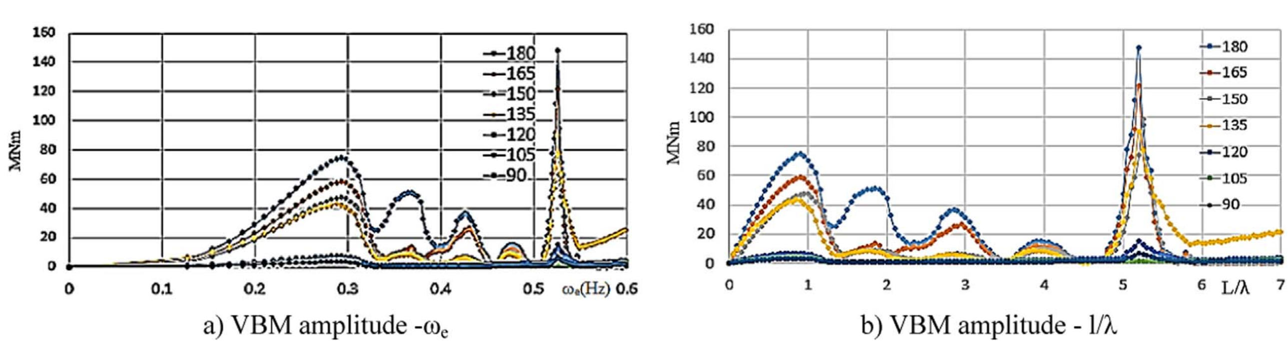

Fig. 19. VBM amplitude of different heading angles.

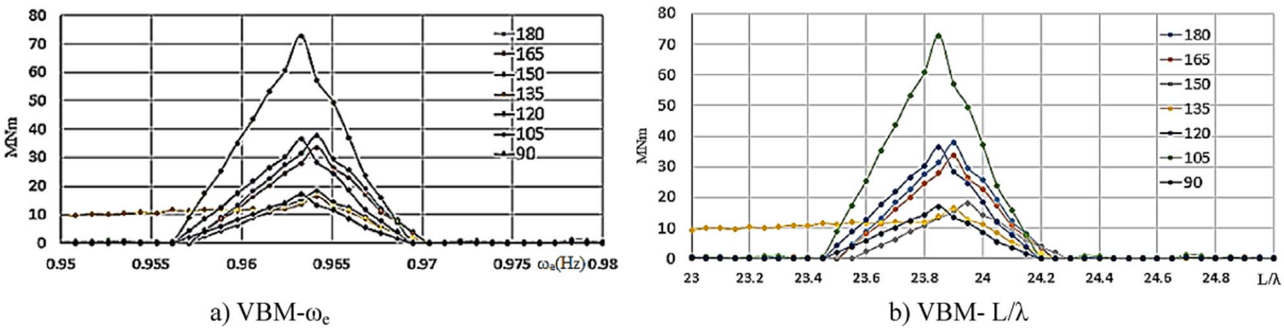

Fig. 20. 1-st order response of VBM of different heading angles.

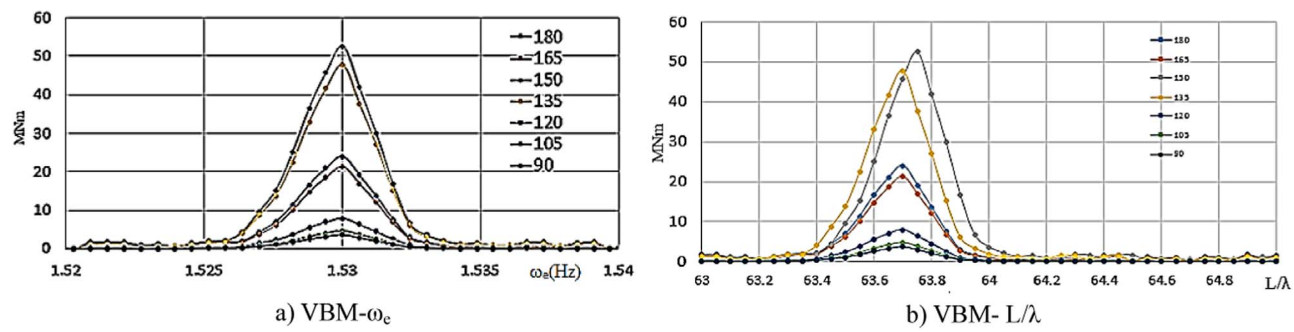

Fig. 21. 2-nd order response of VBM of different heading angles.

Table 4
Spectral analysis assessment results.

Position	North Atlantic				Global				Location
	WM		CM		WM		CM		
	Full load	Ballast	Full load	Ballast	Full load	Ballast	Full load	Ballast	
VS03P3	0.143	0.210	0.165	0.358	0.143	0.210	0.164	0.315	2-n deck corner
VS10P1	0.424	0.451	0.499	0.894	0.384	0.405	0.448	0.648	Hatch corner
VS10P2	0.296	0.259	0.354	0.486	0.296	0.259	0.347	0.384	Upper deck corner

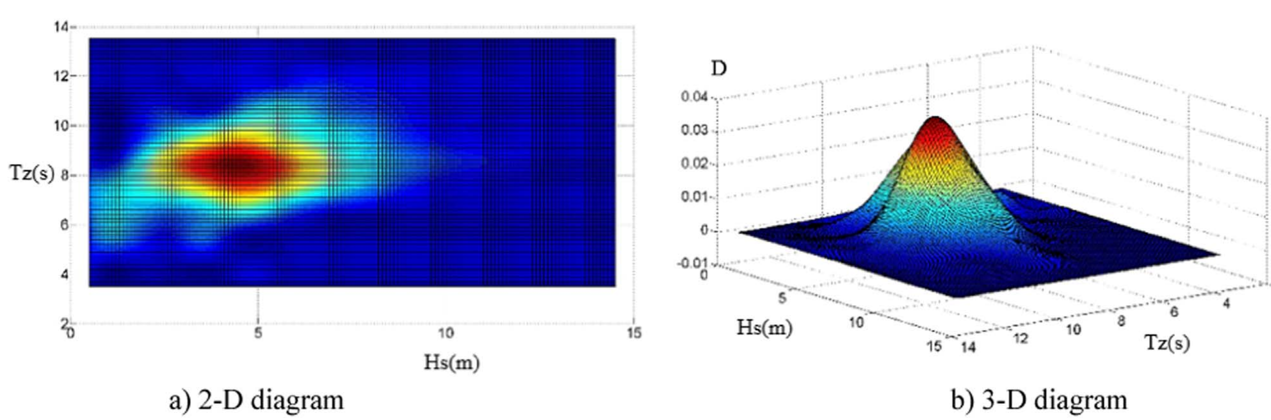

Fig. 22. North Atlantic fatigue distribution diagram of full load condition.

In oblique seas the asymmetric response is calculated to reflect the springing vibration, in the fatigue damage assessment the heading angles are between 0–180° with a step of 15°, here the mid-ship section responses are presented in Fig. 19–21.

From the above results the asymmetric springing response peak values still emerge in the vicinity of the wet natural frequencies, but in different heading angles the VBM amplitudes change from 1-st order to higher order, when the heading angle is 120° the 2-nd order harmonic is the leading factor, and in 105° the 3-rd order harmonic is becoming more significant, at the same time the 1-st order resonance is weakening.

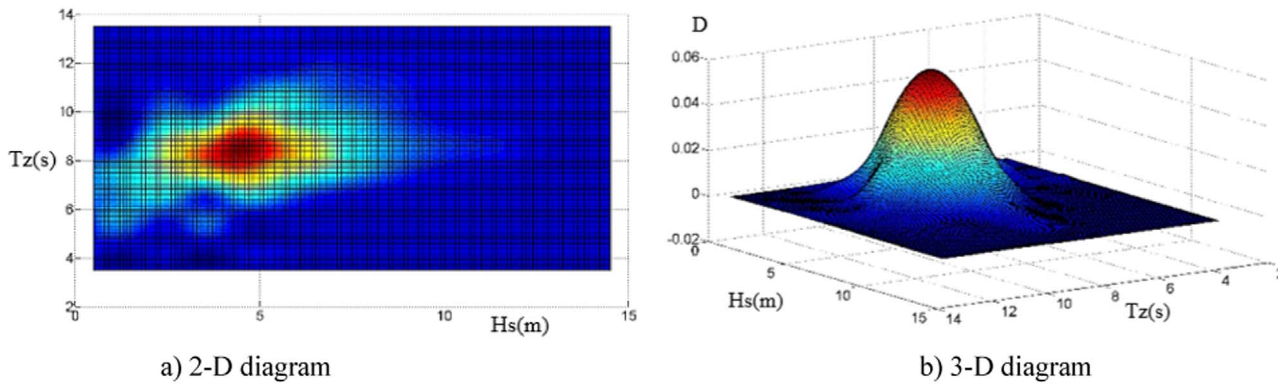

Fig. 23. North Atlantic fatigue distribution diagram of ballast condition.

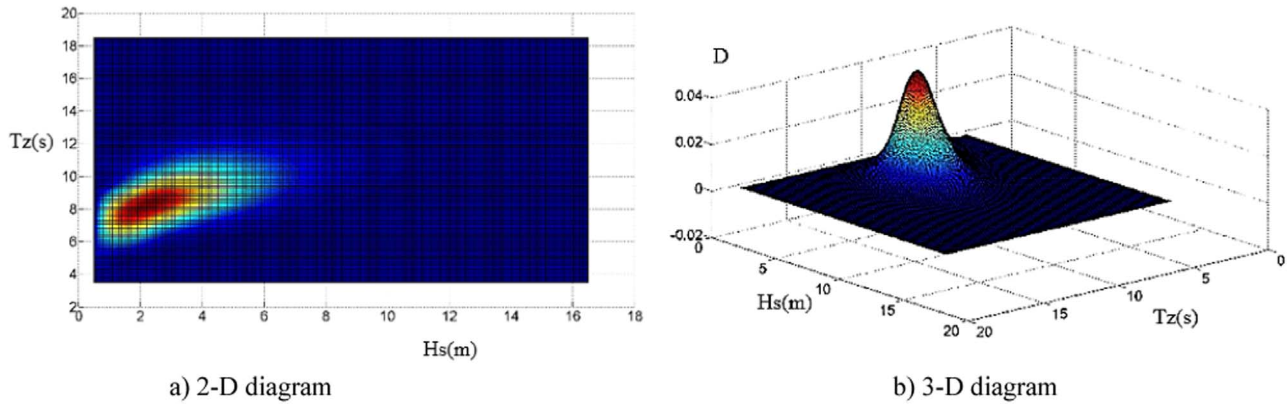

Fig. 24. Global ocean fatigue distribution diagram of full load condition.

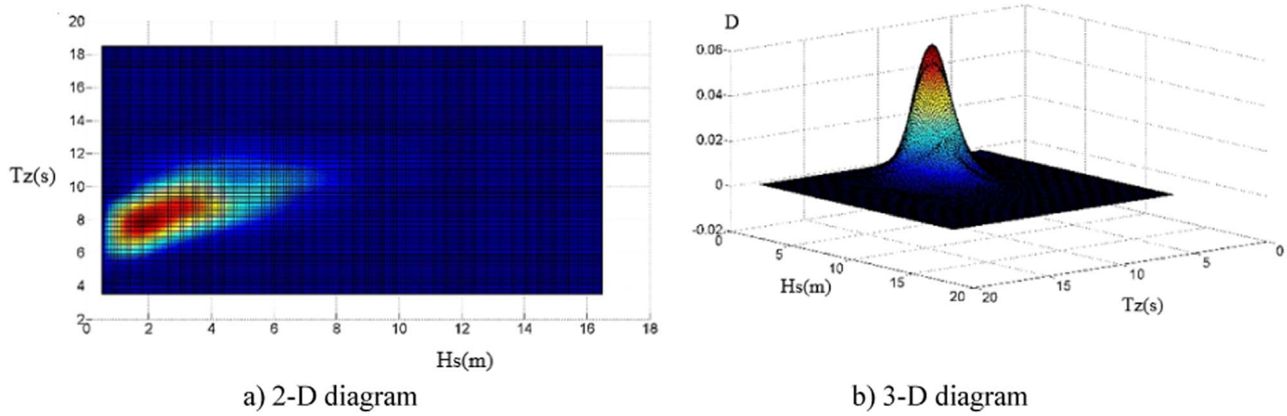

Fig. 25. Global ocean fatigue distribution diagram of ballast load condition.

Table 5
Wave-induced vibration contribution to fatigue damage.

Position	North Atlantic			Global		
	Full	Ballast	Combined	Full	Ballast	Combined
VS03P3	13.22%	41.34%	25.03%	12.56%	33.23%	20.63%
VS10P1	15.07%	49.55%	27.96%	14.21%	37.50%	21.79%
VS10P2	16.41%	46.69%	25.91%	14.80%	32.57%	19.59%

5.4. Fatigue damage assessment

The fatigue damage is based on spectral analysis, the calculation including two loading conditions is according to North Atlantic wave scatter diagram and Global sea wave scatter diagram, the two parameter Pierson-Moskowitz spectrum is used:

$$G_{\eta\eta}(\omega) = \frac{H_s^2}{4\pi}\left(\frac{2\pi}{T_z}\right)^4 \omega^{-5} exp\left[-\left(\frac{2\pi}{T_z\omega}\right)^4/\pi\right] \tag{35}$$

Where $G_{\eta\eta}$ is power spectral density of the wave, Hs is the significant wave height, T_z is crossing zero period.

Weibull distribution is applied as the long term stress range analysis, the accumulate fatigue damage degree is as follows:

$$D = \frac{T_D}{a}\Gamma\left(1 + \frac{m}{2}\right)\sum_{n=1}^{N_{load}} p_n \sum_{i=1}^{n_S}\sum_{j=1}^{n_H} p_i p_j \nu_{ijn}(2\sqrt{2m_{oij}})^m \tag{36}$$

T_d is fatigue life; D accumulate fatigue damage degree; a, m are parameters of S-N curve; N_{load} is loading number; P_n is the n-th loading state proportion; $\Gamma(1 + m/2)$ is gamma function; n_s is sea state number; n_H is the total number of heading angles; p_i is the i-th sea state probability; p_j is the j-th heading angle probability; v_{ijn} is the alternating stress average crossing zero probability ; m_0 is zero order moment.

The results of fatigue damage is related with the stress spectrum, the difference between the stress counting method is great, in this paper the rain flow counting method is applied, which is proposed by Wetzel (1977). In the spectral analysis the calculation is completed according to different heading angles, different significant wave height and different period, here three different positions are chosen to be assessed, the results considering wave-induced vibrations and the results not considering the vibrations are compared, which are shown in Table 4.

The fatigue damage degree of the hatch corner for different wave scatter diagrams are shown in Figs. 22–25:

The final combined results based on the probabilities of the scatter diagram are shown in Table 5:

6. Conclusions

A methodology to predict the fatigue damage of large container ships considering the wave-induced vibrations is presented. The hydroelastic seakeeping program is coupled with the whipping and springing calculations, in which the non-linear fluid forces and hydro-elasticity are included. The air cushion effect is induced in the slamming calculation. The principle values are calculated in detail to predict the symmetric and antisymmetric springing phenomenon. In order to verify the accuracy and effectiveness of this methodology, a 16000TEU container ship is used to calculate the fatigue contributions of springing and whipping in North Atlantic and global wave spectrums.

Through analysis of the fatigue damage by spectral based analysis method, we can see that the long term fatigue damage is closely related with the loading conditions, in the ballast condition the fatigue damage is more serious, when the wave-induced vibrations are considered the fatigue damage will increase significantly, in full load state the fatigue increases about 13%, in ballast condition the incensement up to 40% for North Atlantic sea condition, and more than 30% for global sea condition, the combined results are about 20%.

Storhaug (2007) found that 44% fatigue damage comes from the wave-induced vibrations by means of full scale measurement of a 300 m length ore ship, and for a 13000TEU container ship through 3 h model tests measurement of 19 sea states, the fatigue damage from springing and whipping is up to 65%. Drummen (2008) analyzed the wave-induced vibration contribution to the fatigue damage through model experiment, in which the fatigue life is assumed to be 20 years and 2/3 of the duration is in head waves, the contribution is about 40%, and the vertical bending moment induced by slamming is up to 35%. The results of this paper are consistent with above conclusions, which can verify the reliability of this method.

References

Belgova, M., 1962. Determination of overall bending moments caused by elastic vibrations of ships. In: Transactions of the Leningrad Institute of Water Transport. Issue XXVIII, BSRA Translation No. 1599.

Bereznitski, A., 2003. Local Hydroelastic Response of the Structures Under Impact Loads From Water (Slamming) (Ph.D. Thesis). Delft University of Technology, The Netherlands.

Bisplinghoff, R.L., Doherty, C.S., 1952. Some studies of the impact of wedges on water surface. J. Frankl. Inst. 253, 547–561.

Chuang, S.L., 1966. Experiments on flat-bottom slamming. J. Ship Res. 10 (1), 10–27.

Chuang, S.L., 1970. Investigation of Impact of Rigid and Elastic Bodies with Water. AD702727.

Cleary, W.A., Robertson Jr., J.B., Yagle, R.A., 1971. The Results and Significance of the Strength Studies of the Great Lakes Bulk Ore Carrier Edward L, Ryerson. SNAME Technical and Research Symposium S-2, Ottawa.

Dobrovolskaya, Z.N., 1989. On some problems of similarity flow of fluid with a free surface. J. Fluid Mech. 36 (Part 4), 805–829.

Drummen, I., Storhaug, G., Moan, T., 2008. Experimental and numerical investigation of fatigue damage due to wave-induced vibrations in a containership in head seas. Journal of Marine Science & Technology 13 (4), 428–445.

Drummen, I., 2008. Experimental and Numerical Investigation of Nonlinear Wave-induced Load Effects in Containerships Considering Hydroelasticity (Ph.D. Thesis). Norwegian University of Science and Technology, Oslo.

Eggert, D.I.L., Fricke, D.I.W., Paetzold, D.I.H., 2012. Fatigue strength of thin- plated block joints with typical shipbuilding imperfections. Weld. World Le Soud. Dans Le Monde 56 (11–12), 119–128.

Fabula, A.G., 1957. Ellipse-fitting approximation of two-dimensional normal symmetric impact of rigid bodies in water. In: Proceedings of the Fifth Midwestern Conference on Fluid Mechanics, University of Michigan Press, Ann Arbor, Mich.

Faltinsen, O., 1999. Water entry of a wedge by hydroelastic orthotropic plate theory. J. Ship Res. 43 (3), 180–193.

Fricke, W., Paetzold, H., 2014. Effect of whipping stresses on the fatigue damage of ship structures. Weld. World Le Soud. Dans Le Monde 58 (2), 261–268.

Gu, J., Duan, M., 2016. Integral transform solution for fluid force investigation of a flexible circular cylinder subject to vortex-induced vibrations. J. Mar. Sci. Technol., 1–16.

Hermundstad, O.A., Moan, T., 2005. Numerical and experimental analysis of bow flare slamming on a Ro–Ro vessel in regular oblique waves. J. Mar. Sci. Technol. 10 (3), 105–122.

Hsieh, Shih-Chun, Low, Ying Min, Chiew, Yee-Meng, 2017. Flow characteristics around a circular cylinder undergoing vortex-induced vibration in the initial branch. Ocean Eng. 129, 265–278.

Kahl, A., Rathje, H., Rörup, J., et al., 2013. Semi-empirical assessment of long-term high-frequency hull girder response of containerships. In: Marstruct 2013, International Conference on Marine Structures, pp. 292–297.

Kahl, A., Fricke, W., Paetzold, H., et al., 2014. Whipping investigations based on large-scale measurements and experimental fatigue testing. Int. J. Offshore Polar Eng. 25 (4), 247–254.

Khabakhpasheva, T., Korobkin, A., Malenica, S., 2013. Fluid impact onto a corrugated panel with trapped gas cavity. Appl. Ocean Res. 39, 97–112.

Kim, J.H., Kim, Y., Yuck, R.H., 2015. Comparison of slamming and whipping loads by fully coupled hydroelastic analysis and experimental measurement. Journal of Fluids & Structures 52, 145–165.

Korobkin, A., 2003. Cavitation in liquid impact problems. In: Proceedings of the 5th International Symposium on Cavitation, 1–4 November, Osaka, Japan.

Korobkin, A.A., 2004. Analytical models of water impact. Eur. J. Appl. Math. 6, 821–838.

Korobkin, A.A., 2006. Two-dimensional problem of the impact of a vertical wall on a layer of apartially aerated fluid. J. Appl. Mech. Tech. Phys. 47 (5), 643–653.

Logvinovich, G.V., 1969. Hydrodynamics of Flows with Free Boundaries. Naukova Dumka.

Marine Accident Investigation Branch, 2008. Report on the Investigation of the Structural Failure of MSC NAPOLI English Channel on 18 January 2007 Technical Report.

Moctar, O.E., Ley, J., Oberhagemann, J., et al., 2017. Nonlinear computational methods for hydroelastic effects of ships in extreme seas. Ocean Eng. 130, 659–673.

Miyake, R., Matsumoto, T., Yamamoto, N.. et al. 2010. On the Estimation of Hydroelastic Response Acting on a Ultra-large Container Ship.

Nakos, D.E., 1990. Ship Wave Patterns and Motions by a Three Dimensional Rankine Panel Method (Ph.D. Dissertation). Massachusetts Institute of Technology, USA.

Park, J.B., Song, C.Y., 2015. Fatigue damage model comparison with formulated tri-modal spectrum loadings under stationary Gaussian random processes. Ocean Eng. 105 (3), 72–82.

Rao, Z., Vandiver, J.K., Jhingran, V., 2015. Vortex induced vibration excitation competition between bare and buoyant segments of flexible cylinders. Ocean Eng. 94, 186–198.

Rahaman, M.M., Akimoto, H., 2012. Analysis of the Mechanism of Slamming on the Bow Flare Region of a Container Ship Using RaNS CFD Method.

Semenov, Y.A., Yoon, B.-S., 2009. Onset of flow separation for the oblique water impact of a wedge. Phys. Fluids 21, 112103.

Storhaug, G., 2007. Experimental Investigation of Wave Induced Vibrations and Their Effect on the Fatigue Loading of Ships (Ph.D. Thesis). Norwegian University of Science and Technology, Oslo.

Storhaug, G., Choi, B.K., Moan, T., Hermundstad, O.A., 2010. Consequence of whipping and springing on fatigue for an 8600TEU container vessel in different trades based on model tests. In: Proceedings of the International Symposium on Practical Design of Ships and Other Floating Structures, PRADS2010, Rio De Janeiro, Brazil.

Storhaug, G., Derbanne, Q., Choi, B.K., Moan, T., Hermundstad, O.A., 2011. Effect of whipping on fatigue and extreme loading of a 13000TEU container vessel in bow quartering seas based on model tests. In: Proceedings of the 30th International Conference on Ocean, Offshore and Arctic Engineering, Rotterdam, The Netherlands, OMAE2011-49370.

Tassin, A., Piro, D.J., Korobkin, A.A., Maki, K.J., Cooker, M.J., 2013. Two-dimensional water entry and exit of a body whose shape varies in time. J. Fluids Struct. 40, 317–336.

Tassin, A., Korobkin, A., Cooker, M., 2014. On analytical models of vertical water entry of

a symmetric body with separation and cavity initiation. Appl. Ocean Res. 48 (2014), 33–41.
Von-Karman T., 1929. The Impact on Seaplane Floats during Landing. NACA TN321, Oct.
Vorus, W., 1996. A flat cylinder theory for vessel impact and steady planning resistance. J. Ship Res. 40, 89–106.
Wagner, H., 1931. Landing ofsea planes. NACA Technical Memorandum622.
Wang, E., Xiao, Q., 2016. Numerical simulation of vortex-induced vibration of a vertical riser in uniform and linearly sheared currents. Ocean Eng. 121, 492–515.
Wetzel, R.M., 1977. Fatigue under complex loading: Analysis and experiments for elastic ships. The society of Automotive Engineers, Warrende, PA, USA.
Zhao, R., Faltinsen, O., Aarsnes, J., 1996. Water entry of arbitrary two-dimensional sections with and without flow separation. In: Proceedings of the 21st Symposium on Naval Hydrodynamics.
Zhao, R., Faltinsen, O., 1993. Water entry of two-dimensional bodies. J. Fluid Mech. 246, 593–612.
Zheng, H., Price, R.E., Modarres-Sadeghi, Y., et al., 2014. On fatigue damage of long flexible cylinders due to the higher harmonic force components and chaotic vortex-induced vibrations. Ocean Eng. 88 (88), 318–329.
Zhu, S., Moan, T., 2013. New insight into the wave-induced nonlinear vertical load effects of ultra-large container ships based on experiments. J. Mar. Sci. Technol. 18 (1), 87–114.